coatings

MDPI

Article

# Insulating Thermal and Water-Resistant Hybrid Coating for Fabrics

**Simona Ortelli and Anna Luisa Costa ***

ISTEC-CNR, Institute of Science and Technology for Ceramics–National Research Council of Italy, Via Granarolo 64, I-48018 Faenza (RA), Italy; simona.ortelli@istec.cnr.it

* Correspondence: anna.costa@istec.cnr.it

Received: 22 November 2019; Accepted: 10 January 2020; Published: 14 January 2020


**Abstract:** Organic–inorganic hybrid (ceramer) coatings were synthesized and deposited on the polyester nonwoven fabrics through the sol–gel process. This promoted the formation of an insulating barrier that was able to enhance the thermal stability and the hydrophobicity of fabrics. The hybrid phase is made of an organic network arising from different alkoxysilane precursors (trimethoxymethylalkoxysilane (TMEOS), 3-aminopropyl-trimethoxyalkoxysilane (APTMS), and tetraethylorthosilicate (TEOS)) and inorganic phase made of titanium dioxide $TiO_2$ nanoparticles (NPs) and, in some cases, coated by P-based compound. The characterization of hybrid phase at liquid (size distribution and zeta potential of dispersed nanoparticles), dried state (crystalline phase, thermogravimetric (TGA), and Fourier transform infrared spectroscopic (FTIR) analyses), and on deposited coatings (contact angle, burn-out tests) aimed to find a correlation between the physicochemical properties of ceramer and functional performances of coated fabrics (thermal stability and hydrophobicity). The results showed that all ceramer formulations were able to improve the char formation after burn-out, in particular the highest thermal stability was obtained in the presence of TMEOS precursor and $TiO_2$ NPs coated by P-based compound, which also provided the highest hydrophobicity. In conclusion, we presented an environmentally friendly and easily scalable process for the preparation of ceramer formulations capable of being formed into transparent, thermal-resistant, and hydrophobic fabric coatings, whose functions are extremely challenging for the textile market.

**Keywords:** organic–inorganic hybrid; sol–gel process; ceramer; thermal stability; fabrics

## 1. Introduction

It is well documented that hybrid organic–inorganic materials represent an interesting and up-to-date class of materials with an intrinsic nanostructured morphology, where an organic phase is strictly interconnected with an inorganic one [1,2]. Components making up the hybrids could be molecules, oligomers or polymers, aggregates, and even particles. Therefore, they can be considered composites at the molecular scale. The unique features of hybrids materials do not come from the sum of the individual contributions of both organic and inorganic phases, but from the role exerted by their inner interfaces that become important and predominant [1,3,4]. The hydrolysis and polycondensation of organosilicon compounds with the formation of solid siloxane skeleton $(–O–Si–O–)_n$ has proliferated with silicone chemistry and extended to sol–gel and inorganic chemistry that preferably use as precursors, organically modified alkoxysilanes or metal alkoxides, or even inorganic building units such as clusters or nanoparticles. The resulting hybrid materials form very stable chemical bonds on surfaces [5]. The strong chemical bonding inherent within their siloxane or metal-oxane networks as well as their thermal stability promote inertness against chemical and thermal attack, hence, their potential as protective coatings [6]. Unlike classical nanocomposites,

hybrid organic–inorganic materials have been classified based on cohesion between the two phases (organic and inorganic) provided by strong covalent or iono-covalent bonds (Class I) as well as van der Waals, hydrogen, or ionic bonds (Class II) [7]. The efficiency of these systems could be increased by the addition of nanoparticles (NPs) [8–11]. As a result, organic–inorganic networks that produce dispersed nanostructured phases strictly interconnected are obtained.

The increasing use of synthetic nonwoven fabrics in areas such as agriculture, construction, civil engineering, health care, and in particular the automotive industry [12–15] emphasizes their low thermal stability due to the low melting temperature of their polyester components. The significant recent interest in "green" flame retardant and thermal property enhancer compounds as alternatives to the more common halogen derivatives [16,17] is justified by the negative impact on human health and environment that the latter has showed, with consequent limitations imposed by the current regulatory system [18,19]. Classical "green" alternatives to halogen flame retardant are phosphorous and nitrogen-based compounds [20–23]. Within inorganic green alternatives to halogen-based compounds, metal hydroxides such as aluminum hydroxide and magnesium hydroxide present several positive flame retardant effects if applied as fillers of plastics but only at high loadings (30/60%); however, their application in textile fibres is limited by the need for high filler levels and their large particle size, which is generally of the same order as the diameter of the polymer fibre, with a negative effect on their spinnability [24]. Hybrid organic–inorganic compounds have the possibility to overcome these limitations joining thermal appealing properties of ceramics (inorganic phase) and of organic functional groups, providing a platform for a tailored functionalization of thermally active textile coatings [25–28]. It has been observed, in fact, that the continuous ceramic network of hybrid coatings, based on Si–O–Si linkages in the matrix, acts as a thermal insulator and mass transfer barrier for volatile compounds generated during thermal degradation [29–38], adding another reason for the interest in existing applications in optical, mechanical, biomedical, and electronic fields [2,39–42].

In this work, we exploited sol-gel nanotechnology for preparing organic–inorganic hybrid compositions known as ceramers, and we used them to produce safe and stable fabric coatings with high water fastness, high char-forming efficiency, as well as improved hydrophobic properties. In the specific, ceramer formulations, which differed according to the type of alkoxysilane precursor, the number of NPs and the presence of phosphorus-based compounds were prepared and applied on polyester nonwoven fabrics. The physicochemical properties of different formulations were correlated to wettability and thermal resistance properties of coatings, encouraging the possibility to predict the functional properties of fabrics, thus optimizing the ceramer formulation.

## 2. Experimental

### *2.1. Materials*

The alkoxysilane precursors (trimethoxymethylalkoxysilane (TMEOS), (3-aminopropyl) trimethoxyalkoxysilane (APTMS), and tetraethylorthosilicate (TEOS), whose chemical formula and codes are reported in Table 1, and propan-2-ol (iPrOH), sodium hydroxide (pellets), and hydrochloric acid (all reagent grade) were purchased from Sigma-Aldrich (Italy) and used without any further purification. Sodium polyphosphate $(NaPO_3)_n$, used as P-based compound, was purchased from Riedel-de-Haën$^{TM}$ (Seelze, Germany). Titanium dioxide ($TiO_2$) nanosuspension (NAMA41, 6 wt %, 40 nm), from Colorobbia Italia SpA (Sovigliana Vinci, Italy), was used at different $TiO_2$ concentrations by dilution with distilled water.

**Table 1.** Chemical formulae, name, and code of the (semi) metal alkoxides used as silica precursor in ceramer formulations.

| Chemical Formulae | Name | Code |
|---|---|---|
| 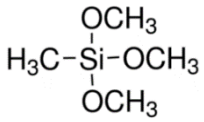 | Trimethoxymethylsilane | (TMEOS) |
| 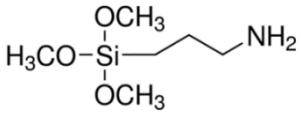 | (3-Aminopropyl)trimethoxysilane | (APTMS) |
| 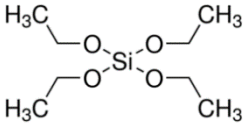 | Tetraethylorthosilicate | (TEOS) |

## 2.2. Ceramer Coating Formation

Ceramer coatings were synthesized and deposited on the polyester nonwoven fabrics through sol–gel process. More specifically, a mixture containing the alkoxysilane precursor (37.2 wt %), distilled water, aqueous nanosuspension containing $TiO_2$ NPs (adding on the bases of different $TiO_2$ content in the final ceramer formulation, see Table 2), and iPrOH (5.1 wt %) were stirred at room temperature for 20 min. The pH was adjusted adding NaOH (10 wt %) or HCl (10 M) solution to reach a value of 4.5. The ceramer suspension precursor was stirred at room temperature for 15 h. Then, the polyester nonwoven fabrics (previously pretreated by water washing for 15 min in ultrasonic bath and then dried in air) were impregnated at room temperature in the mixture solution, for 5 min, passed through a two-roll laboratory padder, and subsequently dried at 100 °C and thermally treated at 130 °C for 30 min in an oven. The step-by-step process is schematized in Figure 1. Finally, all the fabrics were post-washed in distilled water, for 15 min, with ultrasonic bath in order to eliminate the unreacted precursor and not adherent NPs.

Hereafter, the treated polyester nonwoven fabrics will be identified with the code of ceramer formulation, as reported in Table 2.

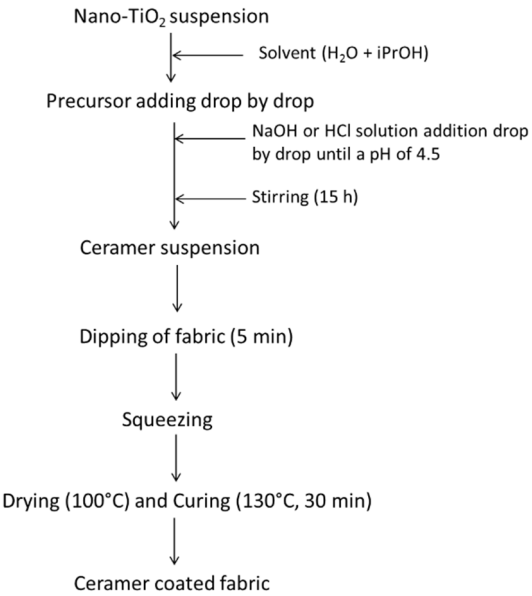


**Figure 1.** Flow chart of sol–gel process used for producing ceramer coated fabrics.

**Table 2.** Main composition characteristics of different ceramer formulations.

| Sample Code | Precursor | $TiO_2$ NPs Content wt % | P-Based Compound Content wt % ** |
|---|---|---|---|
| CERTi4 | TMEOS | 2.3 | 0 |
| CERTi5 | TMEOS | 0.8 | 0 |
| CERTi7 | APTMS * | 2.3 | 0 |
| CERTi8 | TMEOS | 1.2 | 20 |
| CERTi10 | TEOS | 1.2 | 20 |

* APTMS bears an aminopropyl group. ** P-based compound content respect to titanium ($TiO_2$) nanoparticles (NPs) amount.

### 2.3. Characterization of Ceramer Suspensions

The particle size distribution of liquid ceramer formulations was determined by dynamic light scattering (DLS) measurements, performed with a Zetasizer nano ZSP (mod. ZEN5600, Malvern Instruments, Malvern, UK). Hydrodynamic diameter ($d_{DLS}$) includes the coordination sphere; eventual aggregated and agglomerates particles; and the species adsorbed on the particle surface such as stabilizers, surfactants, and so forth. DLS analysis also provides a polydispersion index parameter (PdI), ranging from 0 to 1, quantifying the colloidal dispersion degree; for PdI below 0.2, a sol can be considered monodispersed. Zeta potential ($\zeta$-$pot_{ELS}$) measurements were performed by electrophoretic light scattering (ELS) technique. Smoluchowski equation was applied to convert the electrophoretic mobility to zeta potential. DLS and ELS analyses were carried out on ceramer suspensions diluted (1:10 *v*/*v*) in distilled water. Both particle size distribution and zeta potential analyses were three times repeated, and the data were provided by averaging these measurements with relative standard deviations.

### 2.4. Characterization of Ceramer Powders

The ceramer colloidal formulations were dried at T° = 130 °C for 30 min in oven, obtaining ceramer powders. These powders were characterized by X-ray diffraction (XRD), thermogravimetric (TGA), and Fourier transform infrared spectroscopic (FTIR) analyses. In order to evaluate the thermal behaviour, thermogravimetric analyses (TGA) were carried out on ceramer powders at a heating rate of 10 °C/min up to T° = 600 °C in air flux by thermo-microbalance (STA 449C, Netzsch-Gerätebau GmbH, Selb/Bavaria, Germany). The XRD patterns were obtained on CERTi4, 7 and 10 ceramer powders, as representative samples of each precursor (see Table 1) using a Bragg–Brentano diffractometer (Bruker D8 Advance, Karlsruhe, Germany) operating in a θ/2θ configuration, with an X'Celeretor detector LynkEye (15–75°, 2θ range, 0.02 step size, and 0.5 s per step). The infrared spectra were recorded on CERTi4, 7 and 10 ceramer powders in the wavelength range from 4000 to 300 $cm^{-1}$ using Nicolet 380 FT-IR spectrometer (Thermo Fisher Scientific Inc., Waltham, MA, USA). A powdered sample (approximately 2 mg) was mixed with about 200 mg of anhydrous KBr. The mixture was pressed at 10 Torr pressure into 7 mm diameter disks. A pure KBr disk was used as a blank.

### 2.5. Characterization of Ceramer Coated Fabrics

The amount of material charged on the fabric was quantitatively evaluated by dry add on (AO%), calculated by Equation (1),

$$AO\% = \frac{\left(w_f - w_i\right)}{w_i} \times 100 \quad (1)$$

where $w_i$ = weight before impregnation and $w_f$ = weight after impregnation. The weight measurements were collected using an analytical Sartorius balance ($\pm 10^{-4}$ g).

The presence and the morphology of ceramer coating on polyester nonwoven fabric was investigated by scanning electronic microscopy analysis using field emission scanning electron microscope (FESEM) (Carl Zeiss Sigma NTS-Gmbh, Öberkochen, Germany). The uncoated and coated

polyester nonwoven fabric pieces (about 3 × 3 $mm^2$) were cut and fixed to conductive adhesive tapes and gold metallized. The distribution of elements present in the ceramer coating was measured by image analysis using FESEM coupled to an energy dispersive X-ray micro-analyzer (EDS, mod. INCA Energy 300, Oxford instruments, Oxford, UK).

The wettability was evaluated by the sessile drop method, measuring the static contact angle of a water drop (WCA (°)) on the uncoated or coated fabric surface with an optical tensiometer OCA plus (DataPhysics Instruments, Filderstadt, Germany). For each sample, five measurements were performed and the average value and relative standard deviation were determined.

Burn-out tests were employed to investigate thermal stability at 800 °C with an heating rate of 100 °C/h. The residue (%) was determined weighting each sample before ($w_b$) and after ($w_a$) the heating treatment, according to the following Equation (2):

$$\text{Residue } \% = \frac{(w_a - w_b)}{w_b} \times 100 \quad (2)$$

## 3. Results and Discussion

In the present work, a silica based coating reinforced by $TiO_2$ NPs (ceramer) was applied on fabric, following a design strategy schematized in Figure 2. The main chemical reactions involved in the process were the hydrolysis and the simultaneous condensation in solution (sol) of alkoxysilanes in the presence of ceramic nanoparticles (NPs) until the formation of a three-dimensional network (gel). The amount of material charged on the nonwoven polyester fabrics was about 18 wt.% according to dry add on formula.

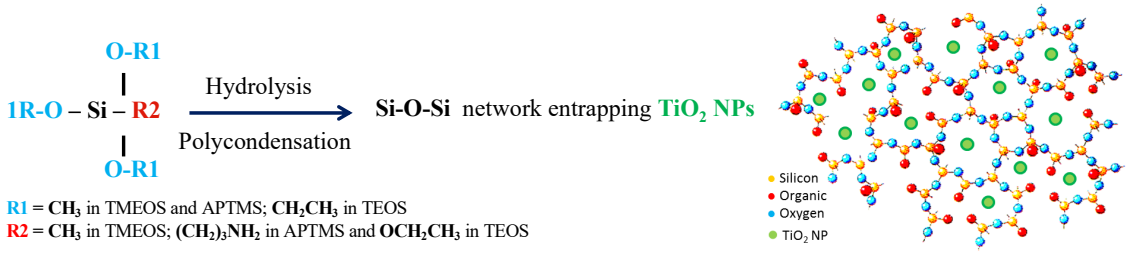


**Figure 2.** Sol–gel design strategy and expected ceramer coating structure.

### *3.1. Ceramer Suspensions*

The ceramer formulations, before applying on fabric, were characterized to identify properties and corresponding functional performances of ceramer coatings. Colloidal characterization of ceramer suspensions showed the formation of aggregates, as the high values of $d_{DLS}$ (Table 3) reveals, if compared with the hydrodynamic diameter of $TiO_2$ NPs (~50 nm [43]). The mean hydrodynamic diameters measured were in the micrometric scale, with the only exception of CERTi7, showing nanometric diameter of about 70 nm, probably because the amino groups of APTMS structure act as dispersing agents that stabilize $TiO_2$ NPs. This is supported by the resulting high and positive $\zeta$-$pot_{ELS}$ value (about +35 mV), which provides an electrostatic repulsion, increasing the natural positive $\zeta$-$pot_{ELS}$ of $TiO_2$ NPs (about +28.5 mV at pH 5.6). Otherwise, the other samples showed relatively low negative $\zeta$-pot data, due to the prevailing contribution of negative Si precursors surrounding $TiO_2$ NPs, justifying the aggregation phenomena and the weak colloidal stability. Data inherent to colloidal characterization of ceramer suspensions are summarized in Table 3.

**Table 3.** Hydrodynamic diameter ($d_{DLS}$), relative polydispersion index parameter (PdI), and zeta potential ($\zeta$-$pot_{ELS}$) of ceramer suspensions.

| | $d_{DLS}$ (nm) | PdI | $\zeta$-$pot_{ELS}$ (mV) |
|---|---|---|---|
| CERTi4 | 1222 ± 138 | 0.2 | −19.8 ± 0.5 |
| CERTi5 | 6932 ± 790 | 0.9 | −14.7 ± 0.2 |
| CERTi7 | 73 ± 0.5 | 0.4 | +34.6 ± 2.2 |
| CERTi8 | 1140 ± 59 | 0.6 | −19.9 ± 0.53 |
| CERTi10 | 1496 ± 187 | 0.8 | −6.0 ± 0.09 |

### 3.2. Ceramer Powders

The ceramer powders were analyzed using thermogravimetric balance. The relative TGA curves are reported in Figure 3. In general, the ceramer powders showed low weight loss. In particular, samples showed a significant thermal stability with values less than 10/15% weight loss. They showed a constant but slight weight loss with increasing temperature, apparently due to surface dehydration and/or dihydroxylation [44], demonstrating the high degree of completeness of hydrolysis/polycondensation process that gives rise to the final ceramer structure. Otherwise, CERTi7, formulation with aminopropyl groups, showed a small weight loss of up to 300 °C due to surface dehydration and a sharp weight loss from 300 °C till 600 °C, with a peak around 400 °C, attributed to decomposition and total loss of the aminopropyl groups from the materials [45]. The higher thermal reactivity of CERTi7 ceramer powder is most likely associated with an incomplete process of formation of the ceramer structure that would justify the decrease of thermal performances of the corresponding coating.

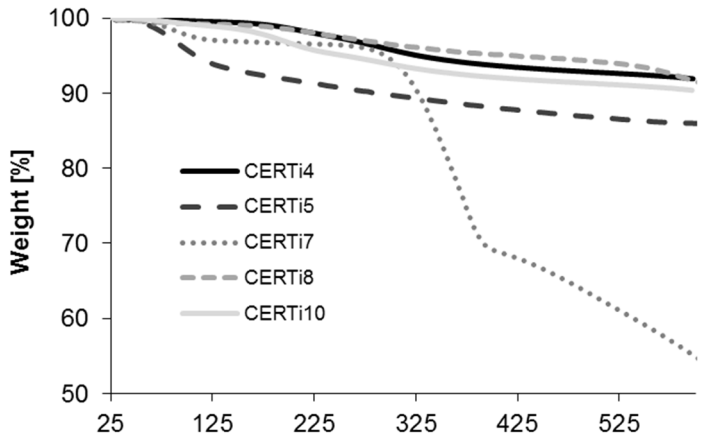


**Figure 3.** Thermogravimetric analysis graphs, showing weight losses of ceramer powders (heating rate of 10 °C/min up to T° = 600 °C in air flux).

Figure 4a shows the XRD patterns of CERTi4, 7, and 10 powders. Anatase is the predominant $TiO_2$ phase, with a small amount of brookite, in agreement with provider technical data sheet [46], having relative peaks more evident in CERTi4 and 10 samples. Moreover, a broad band centered at 2θ = 22°, indicating the characteristic peak of amorphous $SiO_2$ [47] is well visible in CERTi4 and 10 samples. Otherwise, CERTi7 sample showed attenuated peaks in correspondence of crystalline $TiO_2$ phases and amorphous $SiO_2$, probably due to the high organic load still present in the dried powder, as demonstrated by TG analysis. This could justify the broad peak centered at about 2θ = 23° distinguished as "organic hump" [48].

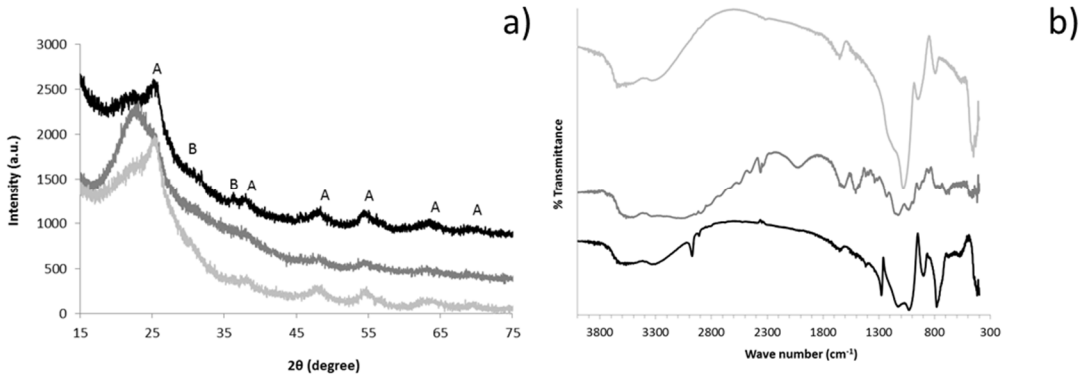


**Figure 4.** X-ray diffractograms (**a**) and Fourier transform infrared spectroscopic (FTIR) spectra (**b**) of CERTi4 (black), CERTi7 (medium gray), and CERTi10 (light gray); (A = anatase; B = brookite).

A deeper analysis of the ceramer functional groups was made by FTIR spectroscopy [49,50], with the resulting spectra being reported in Figure 4b. All samples show peaks, albeit of weak intensity, corresponding to bending vibrations of the $–CH_2$ and $–CH_3$ aliphatic groups around at 1380 and 1450 $cm^{-1}$. The CERTi10 shows peaks in the region 900–1100 $cm^{-1}$ due to $PO_3$ asymmetric and symmetric stretching vibrations, demonstrating the presence of P-based compound. A strong peak near 1090 $cm^{-1}$ is commonly present in IR spectrum of compounds with a –Si–O–C–, whereas an 1190 $cm^{-1}$ band is typical for –Si–O–R– compounds (where R = aliphatic groups), which are clearly visible in CERTi10 spectrum (light gray curve). The CERTi7 shows –C–N– stretching at 1515 $cm^{-1}$, which is not visible in the other samples, and –N–H– vibration region around at 3300 $cm^{-1}$ due to the presence of alkoxysilane hosting aminopropyl groups. Peaks at 1028 and 795 $cm^{-1}$ relating to stretching vibration and symmetrical stretching of –Si–O–Si–, respectively, seen only in CERTi4 spectrum (black curve), are due to the presence of –Si–O–Si– bond from silicate. The broad bands in the region 3000–3600 $cm^{-1}$ are due to the Si–OH groups and moisture. The FTIR analysis seems to confirm that the formation of silica network was more advanced in the CERTi4 ceramer powder, confirming the better performances of TMEOS alkoxysilane precursor.

### *3.3. Ceramer Coating*

The presence of ceramer coating on polyester nonwoven fabrics was confirmed both by add-on value (around 18 wt %) and FESEM images (Figure 5). In fact, FESEM analysis shows the change of surface morphology due to ceramer coatings. In contrast with the smooth texture of the uncoated fiber (Figure 5a), the ceramer coated fibers (Figure 5b–f) show a surface roughness due to the ceramer network entrapping $TiO_2$ NPs. The presence of homogeneously distributed coating was demonstrated also by EDS analyses (Figure 6), mapping the elements distribution. In addition to Si and Ti elements present in all samples, N was detected in CERTi7 sample and P in CERTi8 and CERTi10 samples, in agreement with the precursor components composition. Si maps, perfectly mimicking the texture of fabric, confirmed the uniform distribution of Si surrounding fibers, despite the presence of some cracks. Additionally, Ti, N, and P elements were homogeneously distributed, even with weaker intensity, due to their lower concentration.

The presence of ceramer coatings changed the wettability of polyester nonwoven fabrics, overall improving the hydrophobicity of untreated fabric, with the exception of CERTi7 sample. The improved hydrophobicity could be given by the surface roughening effect, due to the presence of NPs dispersed within ceramer network, as shown by FESEM images in Figure 4. Moreover, as reported in literature, the presence of an extended and uniform siloxane (–Si–O–Si–) network, formed by hydrolysis and condensation of different silica precursors, increases the surface hydrophobicity [51,52]. As reported in Table 4, the contact angle results confirmed that TMEOS (CERTi4 and CERTi8 samples) is the more suitable alkoxysilane precursor for the proposed design strategy, improving the formation of more

compact siloxane network and, as consequence, the associated hydrophobic behavior. The coupling of thermal resistance and water repellency properties are highly desired for many practical applications for multifunctional fabrics. Many products were developed to gain either flame retardancy/thermal stability or hydrophobicity on textile substrates, but few examples [53–55] can boast of both functional properties.

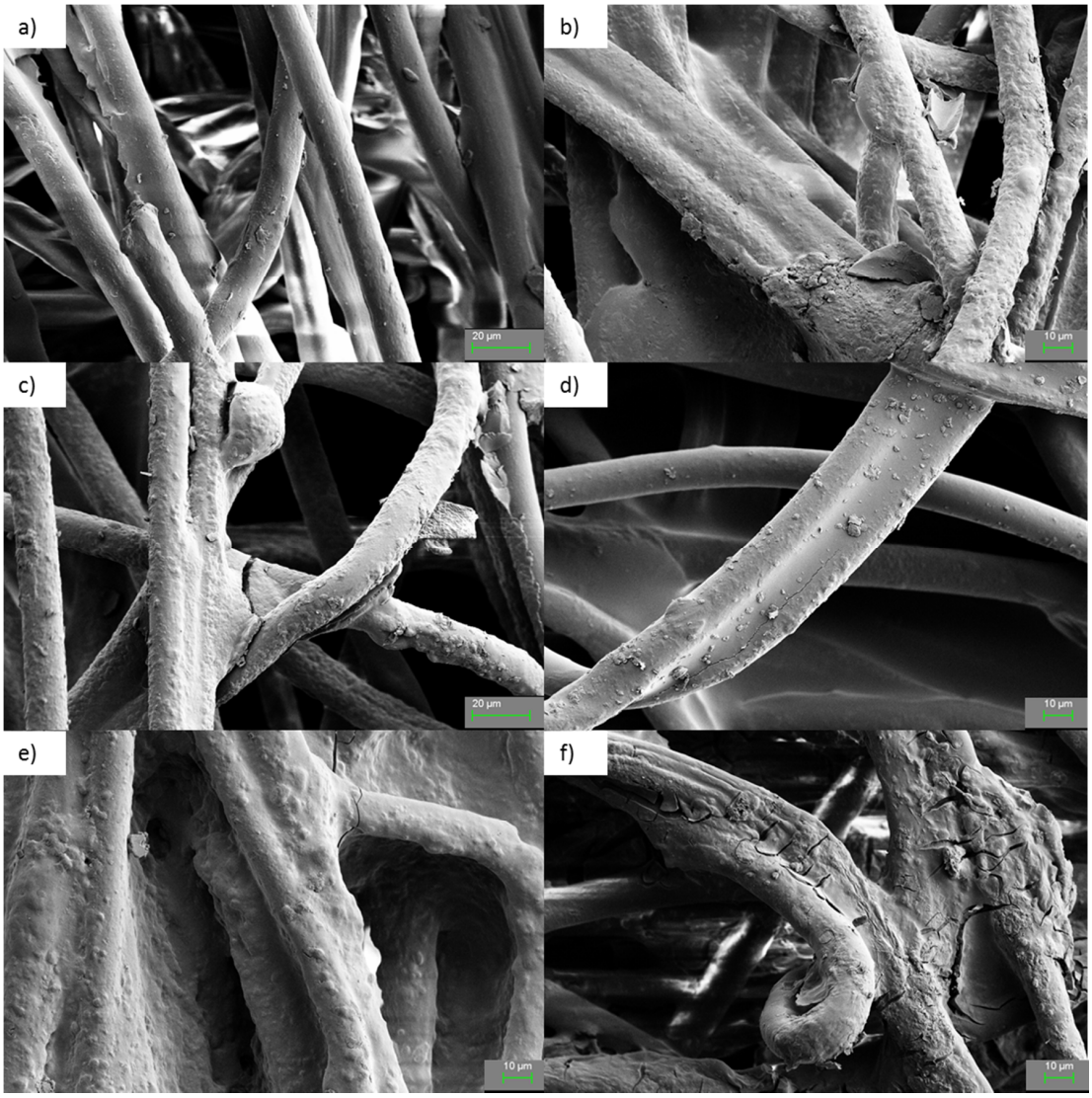


**Figure 5.** Field emission scanning electron microscope (FESEM) images of uncoated fabric fibers (**a**), fabric fibers coated with CERTi4 (**b**), CERTi5 (**c**), CERTi7 (**d**), CERTi8 (**e**), and CERTi10 (**f**).

**Table 4.** Static contact angle with water (WCA) and burn-out test results, expressed as residue% and weight loss% data on different ceramer coated nonwoven polyester fabrics.

| | **WCA (°)** | **Residue% *** | **Weight Loss% *** |
|---|---|---|---|
| Uncoated | 124.06 ± 2.63 | <1 | >99 |
| CERTi4 | 129.01 ± 8.11 | 18.33 | 81.67 |
| CERTi5 | 130.30 ± 14.01 | 1.50 | 98.79 |
| CERTi7 | 85.17 ± 5.45 | 1.35 | 98.50 |
| CERTi8 | 150.95 ± 24.31 | 31.87 | 68.13 |
| CERTi10 | 137.17 ± 10.81 | 15.63 | 84.37 |

* after burn-out test at T° = 800 °C.

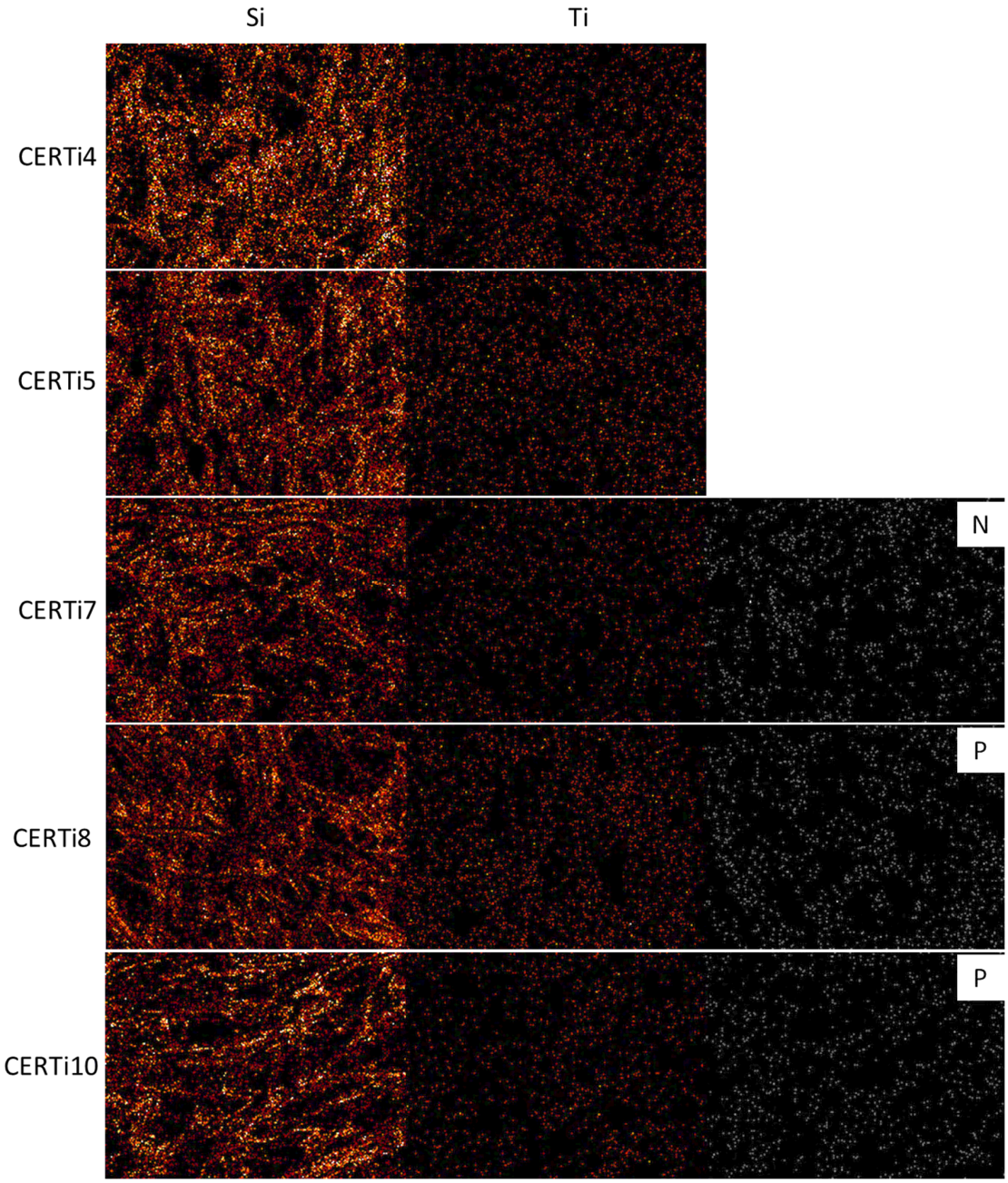


**Figure 6.** FESEM- energy dispersive X-ray micro-analyzer (EDS) maps showing the distribution of Si e Ti elements in the coatings.

The thermal stability in air of ceramer coatings was evaluated by burn-out test, and better performances were attributed to samples with higher burn-out residue. All investigated ceramer coatings substantially increased the thermal stability and promoted char formation, as residues in air at 800 °C confirm (Table 4 and Figure 7 for comparison with un-treated sample). As reported in literature, due to the higher number of hydrolysable groups and the shorter chain lengths of the alkoxysilane precursor, a more uniform silica network is expected with a consequent higher protection against thermal degradation [56]. Comparing the investigated alkoxysilanes, TMEOS, APTMS, and TEOS, it is possible to notice that APTMS sample, despite the presence of amino groups that should reduce the flammability [57], produces the lowest residue. The lowest efficiency of APTMS could be justified by the lower degree of hydrolyzation of the silane chains, most probably due to the decomposition of amino groups that slow down the formation of siloxane network. Comparing TMEOS and TEOS,

differing, respectively, for tetramethoxy or tetraethoxy chain length, we observed that the precursor (TMEOS) with the shortest chain length gives the highest residue, even if has a lower number of hydrolysable groups (three in comparison to four of TEOS). The burn-out results of CERTi8 and 10 samples, which contain P-based compounds, show that, as expected, phosphorus actively contributes to thermal degradation, improving thermal stability [20]; in fact, these samples show the highest residue at 800 °C. Moreover, the contribution of $TiO_2$ NPs should be considered, for their high affinity for Si-based matrix [58] and their capacity to act as physical barrier, promoting the formation of a carbonaceous residue [41] but also for their potential detrimental catalyzing effect, which accelerates the combustions process [59]. Sample CERTi5, which has the lowest amount of $TiO_2$ NPs, showed a very low residue after burn-out, despite the presence of TMEOS precursor. Otherwise, the highest residue of CERTi8 sample (about 32%) is ascribed to the best compromise found between type of silane precursor, amount of $TiO_2$, and presence of P based compound. In any case, it is interesting to know that the thermal stability results of treated fabrics follow the same trend of thermogravimetric analysis performed on ceramer powders, the ceramer samples with lowest weight loss % (CERTi8, 4, and 10) found by TG analysis, showing greatest thermal stability, in terms of residue %, with the following trend: CERTi8> CERTi4> CERTi10> CERTi5> CERTi7. Overall, the good correlation between physicochemical properties (XRD and FTIR) as well as TGA results of ceramer powders and the thermal behavior of ceramer coatings allows one to predict the functional performance of the final material before applying the ceramer suspension on substrate, providing useful information for the design of new creamer coatings.

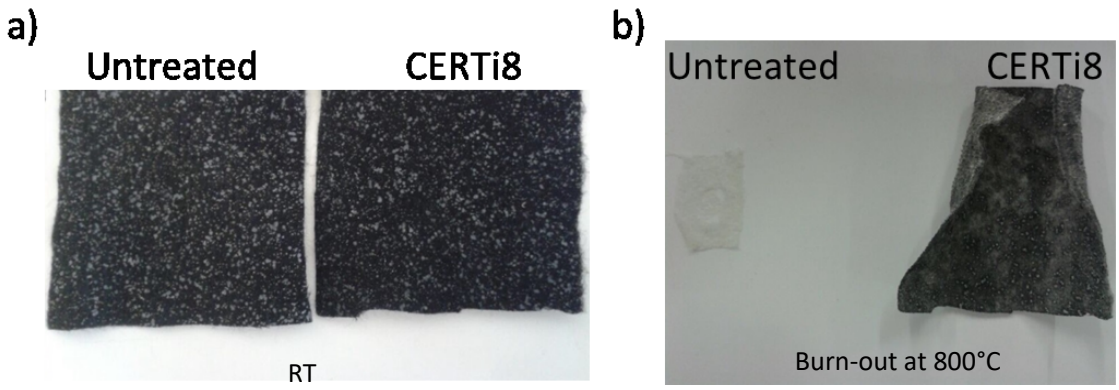


**Figure 7.** Photographs showing the results of burn-out tests: untreated and ceramised fabrics at room temperature (**a**) and after burn-out test at 800 °C (**b**).

## 4. Conclusions

- An environmentally friendly and easily scalable, room temperature, sol–gel process was optimized to apply a ceramer coating on polyester nonwoven fabrics;
- Different ceramer coatings showing an improved thermal stability and enhanced water repellency properties were obtained;
- The results of burn-out tests of ceramised fabrics pointed out that TMEOS precursor characterized by short alkoxy chain length and three hydrolysable groups promotes the formation of the more compact silica-based network, with a homogeneous distribution of elements involved;
- An optimal amount of $TiO_2$ NPs improved the fabrics thermal physical barrier without catalyzing and accelerating the combustion process;
- The addition of P-based compounds in the ceramer formulation improves the thermal stability, whilst the presence of amino groups and their degradation during thermal treatment seems to hinder the formation of a stable and protective –Si-O-Si– network;

- The performances achieved in terms of thermal stability (burn-out residue at 800 °C) were correlated with physicochemical properties of ceramer formulations (composition, FT-IR, and TGA profiles), and a common trend was found between TGA weight losses and burn-out residues;
- The best compromise (highest burn-out residue) was obtained using TMEOS precursor, with an intermediate amount of $TiO_2$ NPs and in the presence of P-based compound;
- The information collected will support the design of new "green" flame retardant and water repellency solutions, which are easily applicable to nonwoven polyester fabrics and usually show a poor affinity for water-based finishing treatments.

**Author Contributions:** Conceptualization, A.L.C. and S.O.; Methodology, S.O.; Investigation, A.L.C. and S.O.; Data Curation, S.O.; Writing—Original Draft Preparation, A.L.C. and S.O.; Writing—Review and Editing, A.L.C. and S.O. Supervision, A.L.C. All authors have read and agreed to the published version of the manuscript.

**Funding:** This research was funded by the European Community's Horizon 2020 Framework Program H2020 (H2020-720851 project PROTECT—Pre-commercial lines for production of surface nanostructured antimicrobial and anti-biofilm textiles, medical devices, and water treatment membranes) (www.protect-h2020.eu).

**Conflicts of Interest:** The authors declare no conflict of interest.

## References

1. Judeinstein, P.; Sanchez, C. Hybrid organic–inorganic materials: A land of multidisciplinarity. *J. Mater. Chem.* **1996**, *6*, 511–525. [CrossRef]
2. Sanchez, C.; Julián, B.; Belleville, P.; Popall, M. Applications of hybrid organic–inorganic nanocomposites. *J. Mater. Chem.* **2005**, *15*, 3559–3592. [CrossRef]
3. Yano, S.; Iwata, K.; Kurita, K. Physical properties and structure of organic–inorganic hybrid materials produced by sol–gel process. *Mater. Sci. Eng. C* **1998**, *6*, 75–90. [CrossRef]
4. Wen, J.; Wilkes, G.L. Organic/Inorganic Hybrid Network Materials by the Sol−Gel Approach. *Chem. Mater.* **1996**, *8*, 1667–1681. [CrossRef]
5. Eduok, U.; Faye, O.; Szpunar, J. Recent developments and applications of protective silicone coatings: A review of PDMS functional materials. *Prog. Org. Coat.* **2017**, *111*, 124–163. [CrossRef]
6. Nazari, M.H.; Shi, X. Polymer-Based Nanocomposite Coatings for Anticorrosion Applications. In *Industrial Applications for Intelligent Polymers and Coatings*; Hosseini, M., Makhlouf, A.S.H., Eds.; Springer International Publishing: Cham, Switzerland, 2016; pp. 373–398. ISBN 978-3-319-26891-0.
7. Sanchez, C.; Belleville, P.; Popall, M.; Nicole, L. Applications of advanced hybrid organic–inorganic nanomaterials: From laboratory to market. *Chem. Soc. Rev.* **2011**, *40*, 696–753. [CrossRef] [PubMed]
8. Norouzi, M.; Zare, Y.; Kiany, P. Nanoparticles as Effective Flame Retardants for Natural and Synthetic Textile Polymers: Application, Mechanism, and Optimization. *Polym. Rev.* **2015**, *55*, 531–560. [CrossRef]
9. Noman, M.T.; Ashraf, M.A.; Ali, A. Synthesis and applications of nano-$TiO_2$: A review. *Environ. Sci. Pollut. Res. Int.* **2019**, *26*, 3262–3291. [CrossRef]
10. Noman, M.T.; Militky, J.; Wiener, J.; Saskova, J.; Ashraf, M.A.; Jamshaid, H.; Azeem, M. Sonochemical synthesis of highly crystalline photocatalyst for industrial applications. *Ultrasonics* **2018**, *83*, 203–213. [CrossRef]
11. Noman, M.T.; Wiener, J.; Saskova, J.; Ashraf, M.A.; Vikova, M.; Jamshaid, H.; Kejzlar, P. In-situ development of highly photocatalytic multifunctional nanocomposites by ultrasonic acoustic method. *Ultrason. Sonochem.* **2018**, *40*, 41–56. [CrossRef]
12. Wang, X.Y.; Gong, R.H.; Dong, Z.; Porat, I. Abrasion resistance of thermally bonded 3D nonwoven fabrics. *Wear* **2007**, *262*, 424–431. [CrossRef]
13. Rwei, S.-P.; Jue, Z.-F.; Chen, F.L. PBT/PET conjugated fibers: Melt spinning, fiber properties, and thermal bonding. *Polym. Eng. Sci.* **2004**, *44*, 331–344. [CrossRef]
14. Ghosh, S.; Villarreal, L. Creating aesthetics and functional values in cotton fabrics through the introduction of thermobonding amorphous polyester fibers into blends. *J. Appl. Polym. Sci.* **2003**, *89*, 3747–3756. [CrossRef]
15. Lin, J.H.; Lou, C.W.; Lei, C.H.; Lin, C.Y. Processing conditions of abrasion and heat resistance for hybrid needle-punched nonwoven bag filters. *Compos. Part Appl. Sci. Manuf.* **2006**, *37*, 31–37. [CrossRef]

16. Schnipper, A.; Smith-hansen, L.; Thomsen, E.S. Reduced combustion efficiency of chlorinated compounds, resulting in higher yields of carbon monoxide. *Fire Mater.* **1995**, *19*, 61–64. [CrossRef]
17. Cireli, A.; Onar, N.; Ebeoglugil, M.F.; Kayatekin, I.; Kutlu, B.; Culha, O.; Celik, E. Development of flame retardancy properties of new halogen-free phosphorous doped $SiO_2$ thin films on fabrics. *J. Appl. Polym. Sci.* **2007**, *105*, 3748–3756. [CrossRef]
18. EC Directive 2002/96/EC on Waste of Electric and Electronic Equipment. *Off. J Eur Union* **2003**, *37*, 24–38.
19. EC Directive 2002/95/EC on Restriction of certain hazardous Substances in Electric and Electronic Equipment. *Off. J. Eur. Union* **2003**, *37*, 19–23.
20. Yaman, N. Preparation and flammability properties of hybrid materials containing phosphorous compounds via sol–gel process. *Fibers Polym.* **2009**, *10*, 413–418. [CrossRef]
21. Rakotomalala, M.; Wagner, S.; Döring, M. Recent Developments in Halogen Free Flame Retardants for Epoxy Resins for Electrical and Electronic Applications. *Materials* **2010**, *3*, 4300–4327. [CrossRef]
22. Apaydin, K.; Laachachi, A.; Ball, V.; Jimenez, M.; Bourbigot, S.; Toniazzo, V.; Ruch, D. Polyallylamine–montmorillonite as super flame retardant coating assemblies by layer by layer deposition on polyamide. *Polym. Degrad. Stab.* **2013**, *98*, 627–634. [CrossRef]
23. Qiu, X.; Li, Z.; Li, X.; Zhang, Z. Flame retardant coatings prepared using layer by layer assembly: A review. *Chem. Eng. J.* **2018**, *334*, 108–122. [CrossRef]
24. Hornsby, P.R. The Application of Fire-Retardant Fillers for Use in Textile Barrier Materials. In *Multifunctional Barriers for Flexible Structure*; Duquesne, S., Magniez, C., Camino, G., Eds.; Springer: Berlin/Heidelberg, Germany, 2007; Volume 97, pp. 3–22, ISBN 978-3-540-71917-5.
25. Kari-Heinz Haas, K. Rose Hybrid inorganic/organic polymers with nanoscale building blocks: Precursors, processing, properties and applications. *Rev. Adv. Mater. Sci.* **2003**, *5*, 47–52.
26. Qian, X.; Song, L.; Hu, Y.; Yuen, R.K.K. Preparation and thermal properties of novel organic/inorganic network hybrid materials containing silicon and phosphate. *J. Polym. Res.* **2012**, *19*, 9890. [CrossRef]
27. Chen, S.; Li, X.; Li, Y.; Sun, J. Intumescent Flame-Retardant and Self-Healing Superhydrophobic Coatings on Cotton Fabric. *ACS Nano* **2015**, *9*, 4070–4076. [CrossRef] [PubMed]
28. Horrocks, A.R. Flame retardant challenges for textiles and fibres: New chemistry versus innovatory solutions. *Polym. Degrad. Stab.* **2011**, *96*, 377–392. [CrossRef]
29. Gao, S.; Shi, Y.; Zhang, S.; Jiang, K.; Yang, S.; Li, Z.; Takayama-Muromachi, E. Biopolymer-Assisted Green Synthesis of Iron Oxide Nanoparticles and Their Magnetic Properties. *J. Phys. Chem. C* **2008**, *112*, 10398–10401. [CrossRef]
30. Lewin, M. Reflections on migration of clay and structural changes in nanocomposites. *Polym. Adv. Technol.* **2006**, *17*, 758–763. [CrossRef]
31. Tang, Y.; Lewin, M. New aspects of migration and flame retardancy in polymer nanocomposites. *Polym. Degrad. Stab.* **2008**, *93*, 1986–1995. [CrossRef]
32. Liu, Y.-L.; Chou, C.-I. The effect of silicon sources on the mechanism of phosphorus–silicon synergism of flame retardation of epoxy resins. *Polym. Degrad. Stab.* **2005**, *90*, 515–522. [CrossRef]
33. Kashiwagi, T.; Gilman, J.W.; Butler, K.M.; Harris, R.H.; Shields, J.R.; Asano, A. Flame retardant mechanism of silica gel/silica. *Fire Mater.* **2000**, *24*, 277–289. [CrossRef]
34. Lewin, M. Some comments on the modes of action of nanocomposites in the flame retardancy of polymers. *Fire Mater.* **2003**, *27*, 1–7. [CrossRef]
35. Cheng, X.-W.; Guan, J.-P.; Yang, X.-H.; Tang, R.-C. Improvement of flame retardancy of silk fabric by bio-based phytic acid, nano-$TiO_2$, and polycarboxylic acid. *Prog. Org. Coat.* **2017**, *112*, 18–26. [CrossRef]
36. Mascia, L. Developments in Organic–inorganic Polymeric Hybrids: Ceramers. *Trends Polym. Sci.* **1995**, *3*, 61–66.
37. Mishra, A.K.; Allauddin, S.; Narayan, R.; Aminabhavi, T.M.; Raju, K.V.S.N. Characterization of surface-modified montmorillonite nanocomposites. *Ceram. Int.* **2012**, *38*, 929–934. [CrossRef]
38. Gou, W.; Che, X.; Yu, X.; Zhang, F.; An, T.; Sun, Y.; Chen, K. Facile fabrication of waterborne fabric coatings with multifunctional superhydrophobicity and thermal insulation. *Mater. Lett.* **2019**, *250*, 123–126. [CrossRef]
39. Nicole, L.; Laberty-Robert, C.; Rozes, L.; Sanchez, C. Hybrid materials science: A promised land for the integrative design of multifunctional materials. *Nanoscale* **2014**, *6*, 6267–6292. [CrossRef]
40. Malucelli, G. Hybrid Organic/Inorganic Coatings Through Dual-Cure Processes: State of the Art and Perspectives. *Coatings* **2016**, *6*, 10. [CrossRef]

41. Ortelli, S.; Malucelli, G.; Cuttica, F.; Blosi, M.; Zanoni, I.; Costa, A.L. Coatings made of proteins adsorbed on $TiO_2$ nanoparticles: A new flame retardant approach for cotton fabrics. *Cellulose* **2018**, *25*, 2755–2765. [CrossRef]
42. Ortelli, S.; Malucelli, G.; Blosi, M.; Zanoni, I.; Costa, A.L. Nano$TiO_2$@DNA complex: A novel eco, durable, fire retardant design strategy for cotton textiles. *J. Colloid Interface Sci.* **2019**, *546*, 174–183. [CrossRef]
43. Ortelli, S.; Costa, A.L. Nanoencapsulation techniques as a "safer by (molecular) design" tool. *Nano-Struct. Nano-Objects* **2018**, *13*, 155–162. [CrossRef]
44. Zhao, J.; Milanova, M.; Warmoeskerken, M.M.C.G.; Dutschk, V. Surface modification of $TiO_2$ nanoparticles with silane coupling agents. *Colloids Surf. Physicochem. Eng. Asp.* **2012**, *413*, 273–279. [CrossRef]
45. Luan, Z.; Fournier, J.A.; Wooten, J.B.; Miser, D.E. Preparation and characterization of (3-aminopropyl)triethoxysilane-modified mesoporous SBA-15 silica molecular sieves. *Microporous Mesoporous Mater.* **2005**, *83*, 150–158. [CrossRef]
46. Ortelli, S.; Costa, A.; Dondi, M. $TiO_2$ Nanosols Applied Directly on Textiles Using Different Purification Treatments. *Materials* **2015**, *8*, 7988–7996. [CrossRef]
47. Ortelli, S.; Poland, C.A.; Baldi, G.; Costa, A.L. Silica matrix encapsulation as a strategy to control ROS production while preserving photoreactivity in nano-$TiO_2$. *Environ. Sci. Nano* **2016**, *3*, 602–610. [CrossRef]
48. Mandile, A.J.; Hutton, A.C. Quantitative X-ray diffraction analysis of mineral and organic phases in organic-rich rocks. *Int. J. Coal Geol.* **1995**, *28*, 51–69. [CrossRef]
49. Edathazhe, A.; Shashikala, H.D. Effect of BaO addition on the structural and mechanical properties of soda lime phosphate glasses. *Mater. Chem. Phys.* **2016**, *184*, 146–154. [CrossRef]
50. Allauddin, S.; Narayan, R.; Raju, K.V.S.N. Synthesis and Properties of Alkoxysilane Castor Oil and Their Polyurethane/Urea–Silica Hybrid Coating Films. *ACS Sustain. Chem. Eng.* **2013**, *1*, 910–918. [CrossRef]
51. Zhang, D.; Williams, B.L.; Shrestha, S.B.; Nasir, Z.; Becher, E.M.; Lofink, B.J.; Santos, V.H.; Patel, H.; Peng, X.; Sun, L. Flame retardant and hydrophobic coatings on cotton fabrics via sol–gel and self-assembly techniques. *J. Colloid Interface Sci.* **2017**, *505*, 892–899. [CrossRef]
52. Xiu, Y.; Hess, D.W.; Wong, C.P. UV and thermally stable superhydrophobic coatings from sol–gel processing. *J. Colloid Interface Sci.* **2008**, *326*, 465–470. [CrossRef]
53. Mohamed, A.L.; El-Sheikh, M.A.; Waly, A.I. Enhancement of flame retardancy and water repellency properties of cotton fabrics using silanol based nano composites. *Carbohydr. Polym.* **2014**, *102*, 727–737. [CrossRef] [PubMed]
54. Xiang, Y.; Pang, Y.; Jiang, X.; Huang, J.; Xi, F.; Liu, J. One-step fabrication of novel superhydrophobic and superoleophilic sponge with outstanding absorbency and flame-retardancy for the selective removal of oily organic solvent from water. *Appl. Surf. Sci.* **2018**, *428*, 338–347. [CrossRef]
55. Bae, G.Y.; Min, B.G.; Jeong, Y.G.; Lee, S.C.; Jang, J.H.; Koo, G.H. Superhydrophobicity of cotton fabrics treated with silica nanoparticles and water-repellent agent. *J. Colloid Interface Sci.* **2009**, *337*, 170–175. [CrossRef] [PubMed]
56. Alongi, J.; Ciobanu, M.; Malucelli, G. Sol–gel treatments on cotton fabrics for improving thermal and flame stability: Effect of the structure of the alkoxysilane precursor. *Carbohydr. Polym.* **2012**, *87*, 627–635. [CrossRef]
57. Alongi, J.; Malucelli, G. State of the art and perspectives on sol–gel derived hybrid architectures for flame retardancy of textiles. *J. Mater. Chem.* **2012**, *22*, 21805–21809. [CrossRef]
58. Gao, T.; Maya-Visuet, E.; He, Z.; Castaneda-Lopez, H.; Zvonkina, I.J.; Soucek, M.D. Effect of pigmentation on polyurethane/polysiloxane hybrid coatings. *J. Appl. Polym. Sci.* **2016**, *133*, 5. [CrossRef]
59. Schartel, B.; Bartholmai, M.; Knoll, U. Some comments on the main fire retardancy mechanisms in polymer nanocomposites. *Polym. Adv. Technol.* **2006**, *17*, 772–777. [CrossRef]


© 2020 by the authors. Licensee MDPI, Basel, Switzerland. This article is an open access article distributed under the terms and conditions of the Creative Commons Attribution (CC BY) license (http://creativecommons.org/licenses/by/4.0/).